




Prediction of Mode I interlaminar fracture toughness of stitched flax fiber composites

M. Ravandi^{1,2,*} , W. S. Teo², M. S. Yong^{1,2}, and T. E. Tay¹

¹Department of Mechanical Engineering, National University of Singapore, 9 Engineering Drive 1, Singapore 117575, Singapore

²Singapore Institute of Manufacturing Technology, Agency for Science, Technology and Research (A-STAR), 2 Fusionopolis Way #08-04, Innovis, Singapore 138634, Singapore

Received: 17 October 2017

Accepted: 21 November 2017

Published online:

27 November 2017

© Springer Science+Business Media, LLC, part of Springer Nature 2017

ABSTRACT

This paper aims to propose a simulation procedure to predict the interlaminar fracture toughness of stitched flax fiber composites through a virtual double cantilever beam test. The proposed procedure is constituted of two steps. First, the interlaminar failure of unstitched flax fiber laminate, as the parent laminate, is modeled using cohesive elements with a nonlinear softening law in order to model the large-scale fiber bridging occurred during delamination. The experimental results are used to calibrate the parameters of the cohesive law. Second, two-node beam elements are superposed onto the cohesive interface of the parent laminate at a prescribed stitch density and distribution to model the bridging stitches present in the validation samples. The stitch material behavior and properties are obtained from the tensile test of impregnated stitch fibers. The out-of-plane flax yarn stitching was found to generate a twofold increase in the delamination resistance of the composite laminate at a medium stitch density. The FE analysis results agreed well with the experimental results, where a good fit between the predicted and experimental R-curves was achieved.

Introduction

In the past decade, the use of natural fibers (NFs) from plants as reinforcement in polymer composites has become more popular thanks to their promising properties such as high-specific stiffness, good acoustic and vibration damping, and eco-friendly characteristics. Despite the attractive properties of natural fibers, the use of these fibers has been more or less limited to the short fiber composites in non-structural applications due to manufacturing

limitations [1–5]. However, recent new fiber extraction methods have been commercially developed to produce long natural fibers with minimum damages induced to the technical properties of the fibers [6, 7].

Numerous studies have confirmed that NFs (such as hemp, flax, and jute) are the most promising alternative of the man-made glass fibers when the mechanical properties per cost and weight come into consideration [8–10]. Among the commonly studied NFs, flax fiber is recognized as one of the high-performance NFs in terms of strength and stiffness per

Address correspondence to E-mail: m.ravandi@u.nus.edu

density, which makes it suitable for a number of structural applications [7, 11–14]. In this regard, similar to man-made fibers, the NFs must be used in the form of continuous unidirectional (UD) or woven textile (with optimally twisted yarns) in the composite laminates so as to utilize the maximum load carrying capacity of the fibers [15, 16]. However, one of the most concerned failure modes is interlaminar failure (namely delamination) in the laminated composites since there is no reinforcement in the thickness direction.

So far, investigations on the man-made composites have come up with various techniques, such as increasing the toughness of matrix, interleaving, engineering the interface adhesion between fiber and matrix, to enhance the interlaminar strength of composites [17–21]. Through-the-thickness stitching of the fiber preforms has been acknowledged as a convenient and cost-effective technique for improving the interlaminar properties [22, 23]. Consequently, a considerable amount of numerical studies have been devoted to model the interlaminar failure of the stitched man-made composite laminates [23–32].

Mai et al. [25] proposed two micromechanics based models to study the effects of stitching on delamination growth of laminate in double cantilever beam (DCB) specimen. In the first model, it was assumed that the stitches are not interconnected at the laminate surfaces, and in the second one, the effect of interconnected stitches was taken into account. The model provided a good understanding of the influence of stitch thread size on the delamination resistance. An analytical model using continuous cohesive spring with linear elastic behavior and brittle fracture was presented by Sankar et al. [33] to simulate crack propagation in stitched composites. The authors concluded that linear modeling is not adequate to predict the interlaminar fracture toughness of the laminates stitched by a strong thread (i.e., Kevlar), where the inelastic behavior of the stitching thread plays a significant role in increasing the toughness. Chen et al. [34] investigated the use of 2-D solid element and 3-D shell element to model parent laminate and bar element to model stitch mechanism to determine the effective Mode I and Mode II fracture toughness of the stitched composites based on the J-integral method. Their study showed that 3-D model is necessary to determine the accurate stress field as well as the stitch interactions with the parent laminate.

Sun et al. [27] used a two-node nonlinear rod element with the micromechanical stitching models introduced in [25] and studied the effect of stitch distribution on improving the delamination resistance by means of virtual crack closure technique (VCCT). In this model, the stitch elements were located between two sub-laminates in which their initial length was zero (before any load was carried by the stitches), and it was assumed that only tension loads can be carried by the stitch elements. A comprehensive study on the effect of stitch distribution has been conducted by Wood et al. [31]. In their study, two-node beam element used in [27] and VCCT has been employed to simulate the DCB test of the stitched composite. Both studies revealed that stitched distribution has significant effect on the critical strain energy release rate (G_{IC}).

Iwahori et al. [29] and Tan et al. [30] developed a 2-D finite element model to simulate the delamination propagation of stitched CFRP for the DCB test by using a three-node rod element to represent a stitch thread. The authors also developed a novel test method to understand the mechanical progressive damage behavior of a single stitch thread (i.e., interfacial deboning, slack absorption, stitch fracture, and frictional pullout) as it is loaded in tension. The results of this test were used as a material model for the stitch elements. The model gave good prediction of the experimental load–displacement curves and critical Mode I strain energy release rates, G_{IC} .

Generally, it is observed that the interlaminar failure of long fiber-reinforced composites happens in the presence of in-plane fiber bridging, which leads to a R-curve development in the fracture energy response [35–37]. The bridging traction of in-plane fibers across the delamination plane of the stitched laminates using high-strength stitch threads is negligible compared to the bridging traction of the out-of-plane stitch fibers. However, the latter has to be taken into consideration when preform stitching is conducted using lower strength materials, like natural fibers [38].

Thus, this study aims to experimentally and numerically investigate the Mode I delamination propagation of stitched natural fiber composite laminates made from continuous UD flax fiber, epoxy polymer, and twistless flax stitching yarns. A 3-D finite element (FE) model of a DCB test specimen was constructed using cohesive element with nonlinear softening law to model fiber bridging effect and the

two-node beam element for the stitch yarn to simulate the effect of bridging stitches and predict the interlaminar fracture toughness in the stitched NF composite.

Methodology

Experimental procedure

Double cantilever beam (DCB) test

The experiments of this study were performed on the composite specimens made of 110 g m^{-2} unidirectional flax fibers FlaxTape™ (LINEO, France) and thermoset resin system Epolam 5051 (Axson, France) with a layup of $[0]_{16}$. The fiber preforms were impregnated with resin by vacuum-assisted resin infusion (VARI) technique at room temperature. As natural fibers tend to absorb moisture due to their hydrophilic nature, the fiber preforms were dried in a vacuum oven for 3 h at $80 \text{ }^\circ\text{C}$ prior to resin infusion. The epoxy mixture was also vacuum degassed for 30 min at room temperature. After resin infusion, the composite was cured at room temperature for 24 h, de-molded, and then post-cured in a convection oven at $80 \text{ }^\circ\text{C}$ for 16 h.

A Tex 250 twistless flax yarn (Composites Evolution, UK) was employed to stitch the fiber preform. Stitching was performed manually with the modified lock stitch pattern, at stitch row spacing of 4 mm and stitch length of 12 mm. To introduce a pre-crack, the front section of the preform was left unstitched to accommodate an $18\text{-}\mu\text{m}$ -thick polytetrafluoroethylene (PTFE) film insert as a crack starter. A schematic illustration of the stitched DCB specimen and the stitch configuration are shown in Fig. 1.

The stitched and unstitched DCB test specimens with a dimension of 20 mm by 170 mm by 4 mm were cut from the composite panels. Three plies of the UD glass fiber were added to both faces of the flax fiber preform prior to resin infusion process to prevent large deformation as well as failure of the specimens' arms. The final thickness of the glass fiber backings (after curing) was measured to be $1 \pm 0.02 \text{ mm}$. Aluminum load blocks were then bonded to the arms of specimens as prescribed by ASTM D5528 [39]. All bonding surfaces were lightly polished, sandblasted, and wiped with acetone-soaked cloth before application of adhesive. The

values of elastic constants used in the modeling of glass composite laminates are summarized in Table 1.

The Mode I DCB tests were performed on an Instron 4505 universal testing machine equipped with a 1-kN load cell, at the crosshead speed of 1 mm min^{-1} , and at least five specimens were tested for each sample. An initial loading–unloading cycle was performed to propagate the crack by 3–5 mm from the pre-crack (PTFE insert) so as to create a naturally sharp crack tip. Then, a second loading–unloading cycle was performed where to propagate the crack by about 60 mm. The crack propagation was monitored visually during the test by means of a traveling microscope, and the crack length was recorded for every 1 mm of crack length increment.

The data reduction method of modified beam theory (MBT), outlined in ASTM D5528, was applied to determine the critical Mode I fracture energy release rate, G_{IC} , as:

$$G_I = \frac{3P\delta}{2b(a + |\Delta|)}, \quad (1)$$

where P is the opening load, δ is the crosshead displacement of the test machine, b is the specimen width, a is the crack length, and Δ is the intercept of the plot of the cube root of the specimen compliance, $\delta \cdot P^{-1}$, against the crack length, a . According to the ASTM standard, the MBT method is recommended since it generally yields the most conservative values of G_{IC} .

Evaluation of tensile properties of the impregnated stitch yarn

The stitch yarn, as a through-the-thickness reinforcement of the composite, will experience tensile loading during the Mode I opening test. It was, therefore, necessary to evaluate the tensile properties of the stitch fibers before and after impregnated with resin. This information is needed to understand the stress–strain contribution of the stitch reinforcements when bridging a crack. The impregnated test specimens were prepared by infusing 25 cm-long dry flax yarns with the same epoxy resin, Epolam 5015, via the VARI technique. The cured, impregnated fibers were tested at a gauge length of 10 mm and the crosshead speed of 1 mm min^{-1} , using an Instron 5500 microtester machine with a 1-kN load cell. The tensile tests were conducted on ten specimens to

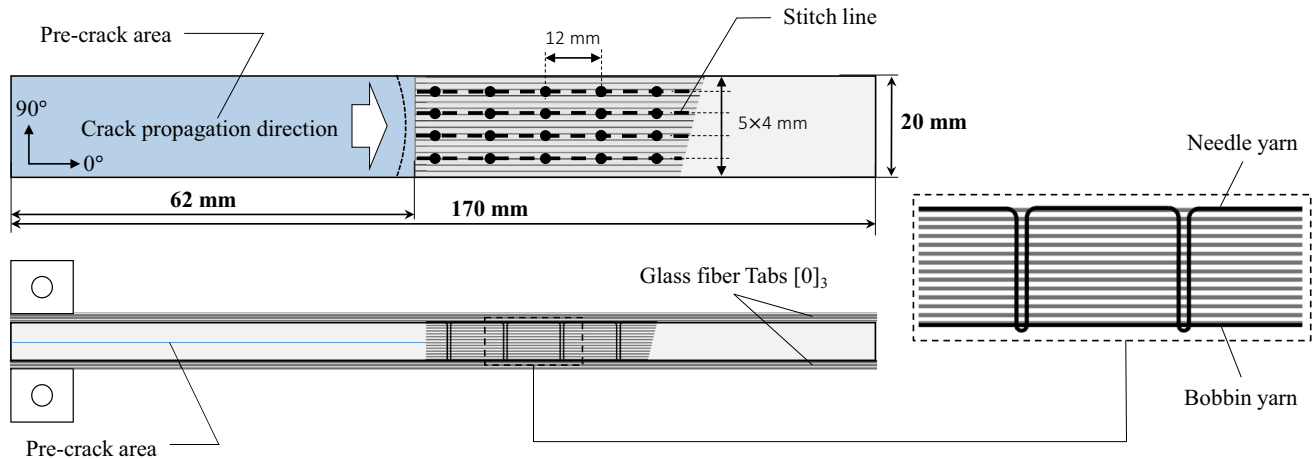


Figure 1 Schematic of the stitched UD flax fiber composite with the stitch parameters.

Table 1 Elastic properties of UD glass composite [36]

Property	Value
Longitudinal modulus, E_{11} (GPa)	47.79
Transverse modulus, $E_{22} = E_{33}$ (GPa)	13.6
Longitudinal shear modulus, $G_{12} = G_{13}$ (GPa)	5.89
Transverse shear modulus, G_{23} (GPa)	5.23
Major Poisson's ratio, $\nu_{12} = \nu_{13}$	0.27
Minor Poisson's ratio, ν_{23}	0.3

assess the variation in the tensile properties of the stitch fibers. The schematic of specimen mounting tab and the tensile test setup for stitch fiber are shown in Fig. 2.

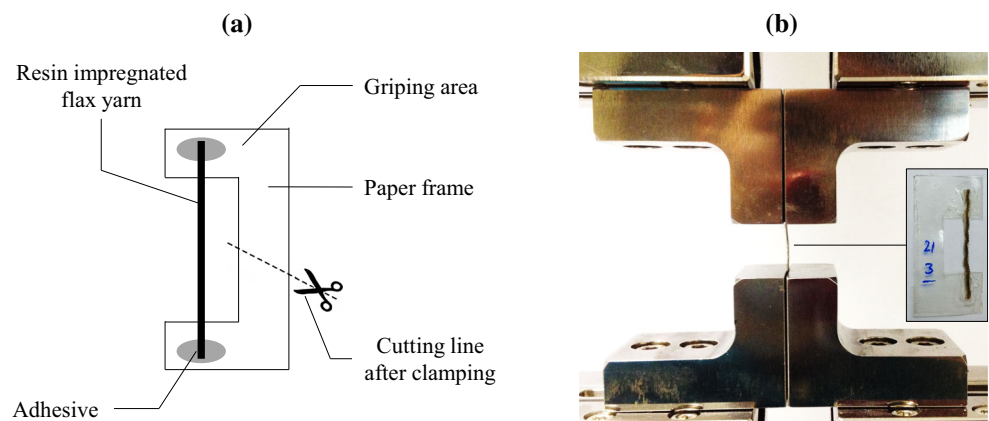
Modeling strategy

The 3-D finite element (FE) model of the DCB test specimen (Fig. 1) used to study delamination in

stitched UD flax composite was created and analyzed using the commercial software Abaqus/Implicit. In the FE model, each arm of the specimen consists of two eight-node quadrilateral in-plane continuum shell elements (SC8R) in the thickness direction to model the UD composites of flax and glass fibers with a layup of $[0_3^{\text{Glass}}/0_8^{\text{Flax}}]_s$, as illustrated in Fig. 3. The midsection interlaminar layer where the two arms are joined is modeled by an eight-node three-dimensional cohesive element with a very small thickness of 0.01 mm. The cohesive elements are connected to neighboring continuum shell elements by sharing nodes.

The boundary conditions are introduced by applying a vertical displacement on the center nodes of the top load block and constraining the center nodes of the bottom load block along the vertical direction. These boundary conditions are according to the DCB experiment where the bottom load block of the specimen is pinned to the fixed jaw, and the

Figure 2 a Schematic view of the mounting tab and b the tensile test of stitch fiber specimen.



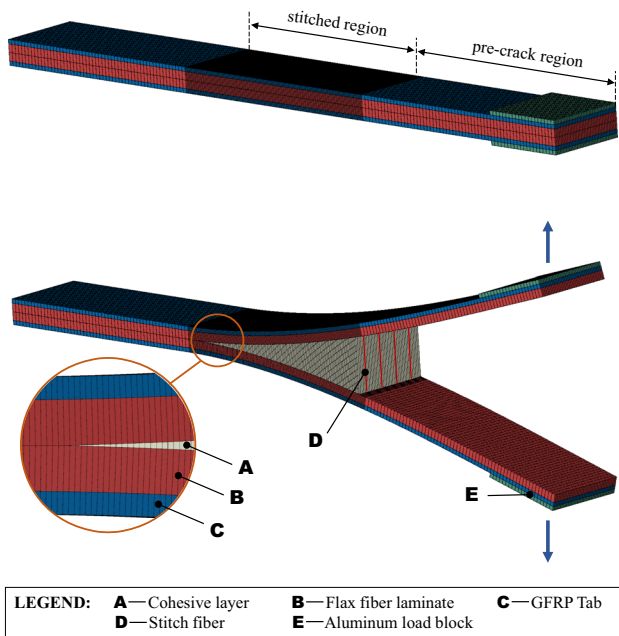


Figure 3 3-D finite element model of the DCB test specimen with a finer mesh at the stitched region.

top load block is pulled using displacement control. An element size of 0.25 mm by 0.5 was used at the stitched region, and a coarse mesh of 1 mm by 0.5 was used for the rest of the specimen. A matched mesh was used for the both continuum element and cohesive element. The element size was determined based on the rule proposed by Harper [44] for the cohesive zone length to ensure that the element is small enough to capture the stress gradient at the wake of crack tips.

To model the interlaminar failure behavior of the stitched flax fiber composite, three fracture mechanisms associated with delamination propagation are considered: (1) decohesion of interlaminar interface (resin-rich layer between the fiber plies) at delamination front, (2) bridging traction of in-plane fibers in the wake of the crack (delamination) tip, and (3) bridging traction of stitch yarns across the delamination plane. The mechanisms (1) and (2) are modeled using trilinear cohesive law, and the mechanism (3) is modeled by introducing beam elements.

The implementation of the model follows two steps. First, the trilinear cohesive law is calibrated using the experimental results of the unstitched UD flax composite. Then, two-node beam element is superposed on the cohesive element to model the stitch fibers, following the distribution shown in Fig. 1.

Delamination

In this study, delamination is modeled using Abaqus cohesive element (COH3D8). A trilinear traction–separation law implemented in a UMAT subroutine is used as the cohesive law. The trilinear cohesive law is used in order to model the R-curve effect of interlaminar fracture toughness of flax fiber composite. According to the author’s previous study [38], this R-curve effect was due to the large-scale in-plane fiber bridging that occurs during delamination propagation. In the presence of an R-curve, the toughness measured during crack propagation increases until reaching a steady-state value. Such response is generally because of involving more than one physical phenomenon in the fracture process, some acting at small opening displacements and others acting at higher opening displacements and extending further into the crack wake. It has been shown that the use of a traction–separation law with a nonlinear softening law is necessary to capture the R-curve effect [35–37, 40, 41].

In this study, the approach proposed by Dávila et al. [36, 37] is applied to the experimental R-curve to determine the parameters of the trilinear cohesive law, i.e., n and m . This trilinear law is obtained from superposition of two bilinear cohesive laws, as shown in Fig. 4. The calibration of the superposition parameters for the UD flax fiber laminate is described in the next section.

The cohesive tractions ($\sigma_n, \sigma_s, \sigma_t$) are related to the corresponding separations in the normal and shear directions ($\delta_n, \delta_s, \delta_t$) thru Eq. (2):

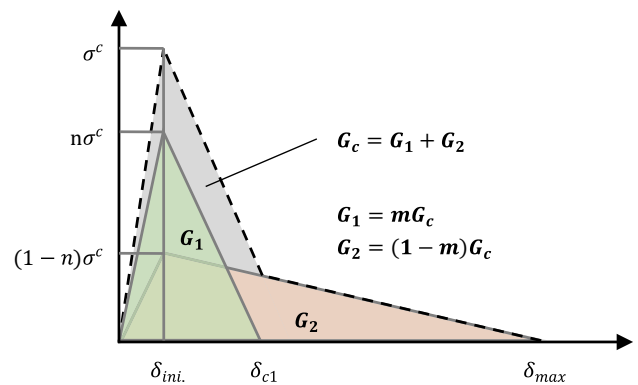


Figure 4 Superposition of two bilinear cohesive laws and resultant trilinear cohesive law (reproduced from [36]).

$$\begin{bmatrix} \sigma_n \\ \sigma_s \\ \sigma_t \end{bmatrix} = \begin{bmatrix} D_{nn} \left(1 - \frac{\langle \delta_n \rangle}{|\delta_n|} d \right) & 0 & 0 \\ 0 & D_{ss}(1-d) & 0 \\ 0 & 0 & D_{tt}(1-d) \end{bmatrix} \begin{bmatrix} \delta_n \\ \delta_s \\ \delta_t \end{bmatrix}, \tag{2}$$

in which D_{nn} , D_{ss} , and D_{tt} are the penalty stiffness, and d is the damage variable ($d = 0$ for when there is no damage in the interface and $d = 1$ once the interface is completely fractured) [42]. The $\langle \cdot \rangle$ in Eq. (2) is Macauley bracket operator, which is defined for every $\alpha \in \mathbb{R}$ as $\alpha = \frac{(\alpha + |\alpha|)}{2}$. In other words, the damage variable does not influence the σ_n when crack is closed in compression. In Eq. (2), the penalty stiffnesses D_{nn} , D_{ss} , and D_{tt} are artificial parameters used to constrain the separation (or interpenetration) between the crack faces and have perfect bonding between plies before delamination onset. Therefore, they must be large enough compared to the stiffness of the lamina [43–45]. Here, the formulas of Eq. (3) are employed to calculate the minimum values of the penalty stiffness [44]

$$D_{nn}^{\min} = \frac{50E_3}{t_p}, D_{ss}^{\min} = \frac{50G_{13}}{t_p}, D_{tt}^{\min} = \frac{50G_{23}}{t_p}, \tag{3}$$

where E_3 , G_{13} , and G_{23} are the elastic modulus of the lamina and t_p is the thickness of a single ply. The values of the material parameters used are given in Table 2.

Delamination onset is modeled using the quadratic failure criterion as:

$$\left(\frac{\sigma_n}{\sigma_n^c} \right)^2 + \left(\frac{\sigma_s}{\sigma_s^c} \right)^2 + \left(\frac{\sigma_t}{\sigma_t^c} \right)^2 = 1, \tag{4}$$

in which σ_n , σ_s , and σ_t are the normal and shear stresses on the interface and σ_n^c , σ_s^c , and σ_t^c are the

Table 2 Material properties for UD flax fiber composite

Property	Value
Longitudinal modulus, E_{11} (GPa)	25.3
Transverse modulus, $E_{22} = E_{33}$ (GPa)	4.1
Longitudinal shear modulus, $G_{12} = G_{13}$ (GPa)	3.4 ^a
Transverse shear modulus, G_{23} (GPa)	2.8 ^a
Major Poisson’s ratio, $\nu_{12} = \nu_{13}$	0.25
Minor Poisson’s ratio, ν_{23}	0.3 ^a
Mode I interlaminar fracture toughness, G_{IC} (kJ m ⁻²)	1.25
Normal strength of the interface, σ_n^c (MPa)	35

^aEstimated value

normal and shear strengths of the interface [46]. Once Eq. (4) is satisfied, delamination is initiated. Then, interface damage evolution is specified based on a fracture energy criterion and the bilinear softening law:

$$\int_0^\infty \sigma_{\text{eff}} d\delta_{\text{eff}} = G_C, \tag{5}$$

in which σ_{eff} and δ are the effective traction and displacement, respectively, and G_C is the fracture energy [47]. The material properties used in the delamination failure criterion are given in Table 2.

Modeling of stitching yarns by beam elements

According to the experimental observations, following assumptions are made as a basis for the stitch model [48]:

- The stitch yarns are cylindrical with circular cross section.
- The stitch yarns only carry tensile load.
- The failure of stitch yarns is brittle-like failure (fiber failure) under tension.
- The breakage of stitch yarns is assumed to occur at the delamination plane.
- No slippage occurs at the embedded stitches (i.e., no stitch pullout).
- The tensile properties of the stitch yarns are obtained from the tensile test of impregnated stitch yarns.

The SEM of a delaminated surface of the flax yarn stitched UD and woven flax fiber composite associated with the assumptions (D) and (E) is shown in Fig. 5.

The crack bridging traction of through-the-thickness stitch reinforcements is modeled using two-node beam elements with a brittle fracture response, implemented in a UMAT subroutine. A maximum longitudinal stress failure criterion was used to determine fiber failure under tension. The material properties used in the modeling of the stitch fibers are given in Table 3. In this study, the material properties of the flax fiber laminate and its interlaminar fracture toughness were empirically determined from the tensile and DCB test results, and the elastic properties of the glass fiber laminates were adapted from literature [36].

Figure 5 SEM of the delaminated surface for the DCB test specimen of **a** UD and **b** woven flax fiber composite, illustrating fractured stitch (flax) yarn at delamination surface with minimum occurrence of slippage and fiber pullout.

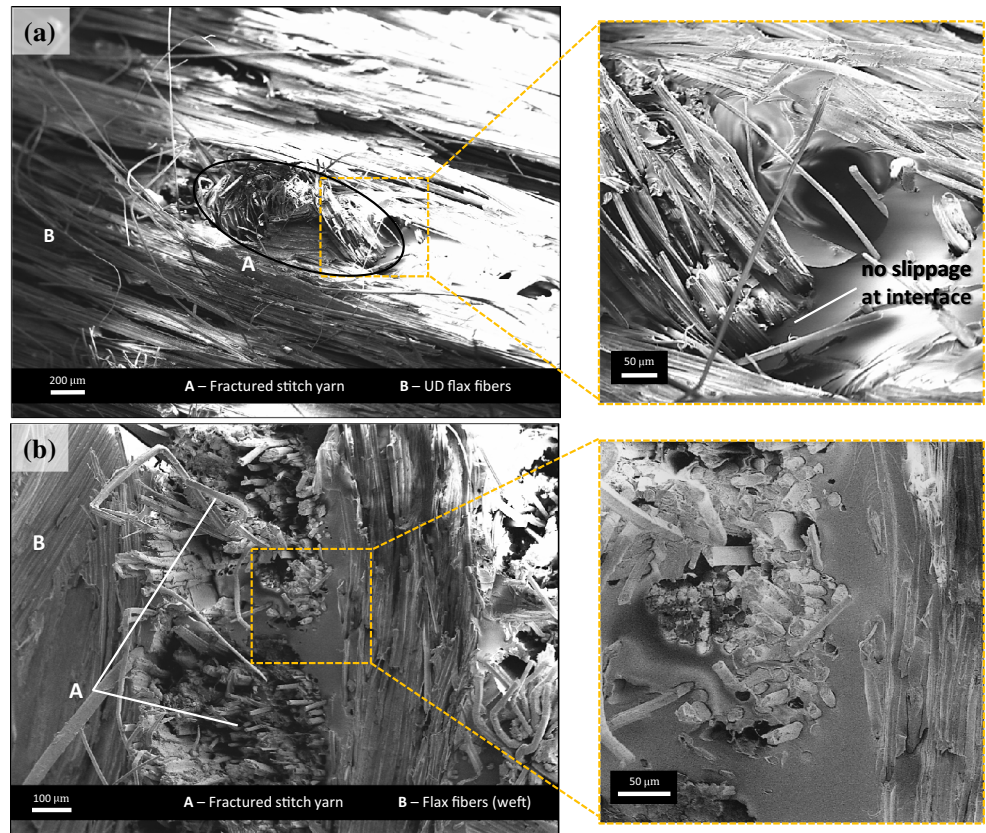


Table 3 Material properties of flax yarn as stitch fiber

Property	Value
Longitudinal modulus, E_1 (GPa)	38.97
Longitudinal tensile strength, X_t^{stitch} (MPa)	330
Elongation at break, ϵ (%)	3.7
Stitch cross-sectional area, A^{stitch} (mm ²)	0.33

Results and discussion

Modeling of in-plane fiber bridging by means of cohesive law

In this section, the trilinear cohesive law (Fig. 4), which is being obtained from superposition of two linear softening laws, is calibrated to capture the delamination crack propagation in the presence of fiber bridging. A semi-analytical approach proposed [36] is applied to the DCB test results, i.e., R-curves, of the unstitched UD flax fiber composite to determine the parameters of the superposed cohesive laws.

Testing for fracture properties of unstitched composite

The G_{IC} values obtained from the DCB tests of the unstitched UD flax fiber composites in relation to the change in crack length, Δa , during crack propagation are presented in Fig. 6. In addition to the modified beam theory (MBT) method, the G_{IC} values determined from the compliance calibration (CC) and the

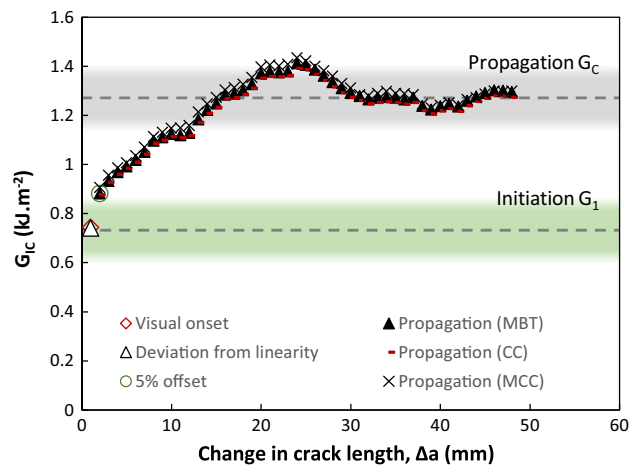


Figure 6 Measured G_{IC} values of the unstitched UD flax/epoxy composite versus crack length (R-curve).

modified compliance calibration (MCC) methods [39] were also plotted to check for differences in the calculation of G_{IC} values through the use of different data reduction methods. It was observed that these three methods, which are all based on the relation of Irwin–Kies for strain energy release rate [49], led to a very similar G_{IC} values with a maximum variation of 2.5%. Since the analysis is robust and the MBT analytical corrections, as the most conservative method, work just as well for the stitched composites, the G_{IC} values reported and used for simulation in this study are all calculated based on the MBT method.

From the DCB test results of the unstitched flax composite, it was observed that the interlaminar fracture toughness rose steadily with increasing (delamination) crack length as the crack propagated in steady state. In general, such a response, which is often referred to as the resistance curve or R-curve, indicates the involvement of different physical phenomena occurring in tandem during the fracture process. The R-curve association with fiber bridging is a well-established phenomenon [50], and the slow rise in fracture resistance of the flax/epoxy specimens up to the first peak G_{IC} value at $\Delta a \approx 25\text{--}30$ mm (Fig. 6) agrees with our experimental finding of a large natural fiber bridging zone that visually measured up to 25–30 mm in length when it was fully developed, as shown in Fig. 7. So, the R-curve effect is attributed to the increase in apparent

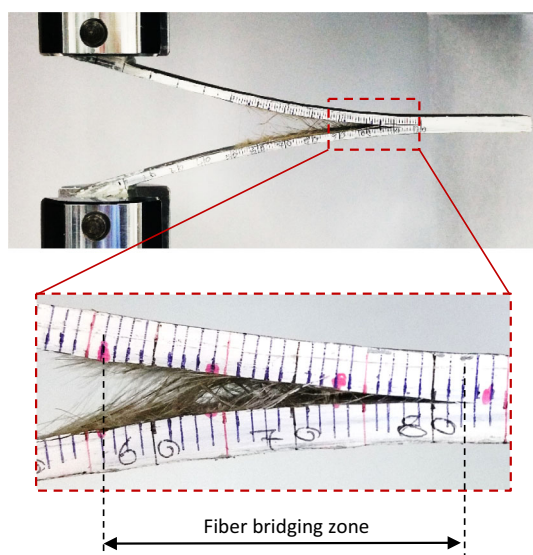


Figure 7 In-plane fiber bridging across the delamination plane of UD flax fiber composite during DCB test.

stiffness and delamination resistance of the specimen as a result of fiber bridging.

The large-scale fiber bridging is believed to be a unique characteristic of untwisted UD natural fiber composites, as the preform architecture allows the elementary natural fibers to behave in a way similar to discontinuous aligned long fibers. The long bridging zone could also explain why the interlaminar fracture toughness of the flax composite is significantly higher than that measured for glass fiber composites (671 J m^{-2}) [38]. It is therefore essential to consider the effect of fiber bridging in the FE delamination model for natural fiber composites, in order to achieve a more accurate prediction of their strength and fracture behavior.

The experimental results show that the average initiation value of G_{IC} for the UD flax/epoxy composite is 0.771 kJ m^{-2} and the steady-state G_{IC} value is 1.25 kJ m^{-2} which is reached after approximately 25–30 mm of crack propagation. The length of crack propagation before the steady-state phase of Mode I critical strain energy release rate was estimated based on the mean value of the steady-state G_{IC} with a 95% confidence interval (for upper and lower limits).

Superposition of cohesive laws for modeling the effect of fiber bridging

The trilinear cohesive law (bilinear softening) of Fig. 4, obtained from superposition of two bilinear cohesive laws, is employed to model the fiber bridging effect encountered during Mode I fracture of UD flax fiber composites. Accordingly, a semi-analytical relation for extracting the superposition parameters of the cohesive laws from the experimentally obtained R-curves is used [36]. In this method, two bilinear cohesive laws with their own specific characteristics are superposed to obtain a trilinear cohesive law. The superposition parameters of m and n (Fig. 4) are defined as follows:

$$\begin{aligned} G_1 &= mG_c, G_2 = (1 - m)G_c \\ \sigma_1 &= n\sigma_c, \sigma_2 = (1 - n)\sigma_c \end{aligned} \quad (6)$$

where σ and G refer to the cohesive strength and Mode I fracture toughness, respectively. According to the experimental R-curve of the UD flax fiber composites (Fig. 6), the average initiation value of Mode I critical strain energy release rate (G_1) was 0.771 kJ m^{-2} and the steady-state value (G_c) was 1.25 kJ m^{-2} , which was reached after approximately 25–30 mm of crack

propagation. Thus, the first relation of Eq. (6) leads to $m = G_1/G_c = 0.616$. In order to identify the other parameter, n , it is necessary to establish a relationship between the characteristic length of the process zone for the trilinear cohesive law (l_{c_Sup}) and the characteristic length of each primary bilinear cohesive law, $l_{ci}, i = 1, 2$. There are special cases in the relation between the characteristic length of the process zone for the trilinear and the primary bilinear laws [36]. These special cases are as follows:

1. The sum of two bilinear laws is a bilinear law when $m = n$.
2. If one of the two bilinear cohesive laws has no associated fracture toughness (i.e., either $m = 0$ or $m = 1$), the contribution of that particular cohesive law is neglected.
3. If the strength of a bilinear cohesive with a nonzero fracture toughness tends to zero (i.e., either $n \rightarrow 0$ or $n \rightarrow 1$), the superposition process zone will tend to infinity.
4. The order of the superposition of the two bilinear laws is irrelevant.

These special cases for the length of process zone of the trilinear cohesive law (l_{c_Sup}) can be stated as:

$$\begin{aligned} l_{c_Sup}(n, n) &= l_c \\ l_{c_Sup}(n, m = 0) &= l_{c2} \\ l_{c_Sup}(n, m = 1) &= l_{c1} \\ \lim_{n \rightarrow 0 \text{ or } 1} l_{c_Sup} &= \infty \end{aligned} \tag{7}$$

$$l_{c_Sup}(n, m) = l_{c_Sup}(1 - n, 1 - m)$$

The characteristic length of the process zone for the trilinear cohesive law (l_{c_Sup}), based on the superposition parameters m and n , can be calculated using the following interaction equation [36]

$$l_{c_Sup}(n, m) = \left[\frac{m^2}{n^2} + \left(\frac{1 - m}{1 - n} \right)^2 - \frac{m(1 - m)}{n(1 - n)} \right] l_c, \tag{8}$$

in which all the conditions of Eq. (7) are satisfied. In Eq. (8), l_c is the material characteristic length, which is an intrinsic fracture property of material. The characteristic length l_c is usually estimated as [37]

$$l_c = \gamma \frac{E'G}{\sigma_c^2}, \tag{9}$$

where G and σ_c are the fracture toughness and strength of the material, respectively. The modulus E' under plane stress condition is defined as

$$E' = 2E_{22} \left(\sqrt{2 \left[\sqrt{\frac{E_{22}}{E_{11}}} - \nu_{21} \right] + \frac{E_{22}}{G_{12}}} \right)^{-1}, \tag{10}$$

where ν_{21} is the in-plane Poisson’s ratio and E_{22} and G_{12} are the transverse Young’s modulus and shear modulus, respectively. In Eq. (9), γ is a non-dimensional parameter and depends on the damage/yielding process. In general, the length of process zone under steady-state propagation is estimated by the characteristic length ($l_{pz}^{ss} \approx l_c$). However, the estimation is valid only when the material characteristic length l_c is smaller than the structural dimension. This is because the value of γ in Eq. (9) is noticeably influenced by the structural dimension. Therefore, considering the effect of structural thickness is essential in prediction of the steady-state process zone length. Thus, the empirical relation of Eq. (11) proposed by [36] was used to apply thickness correction on the characteristic length obtained from Eq. (8) for the superposed cohesive law, l_{c_Sup} , as

$$l_{pz_Sup}^{ss} = \left(\frac{t_{arm}}{t_{arm} + l_{c_Sup}} \right)^\beta l_{c_Sup}, \tag{11}$$

where t_{arm} is the block thickness (thickness of plies stacking with same orientation) and β is a non-dimensional parameter. Nonlinear Eq. (11) can be solved for l_{c_Sup} , in which $t_{arm} = 2.99\text{mm}$ and the steady-state process zone length is $l_{pz_Sup}^{ss} = 30\text{mm}$ (estimated from experimental R-curve). Finally, using the calculated values of parameter m and l_{c_Sup} , the nonlinear Eq. (8) can be solved for the parameter n iteratively, which results $n = 0.9699$.

FE modeling of DCB test of unstitched composite

The trilinear cohesive law using the calculated values of $n = 0.9699$ and $m = 0.6160$ was applied to the cohesive elements of the FE model of the DCB specimen. The force–displacement responses of the DCB test specimen model of unstitched UD flax fiber composite using bilinear and trilinear cohesive laws, compared to the experimental data, are shown in Fig. 8. It can be clearly seen that the prediction with the linear softening law is not suitable for modeling the interlaminar fracture of the UD natural fiber composite. When the initiation value of G_{IC} is used [denoted by ‘FEM-Bilinear law ($G_{IC} = 0.77$)’], the delamination

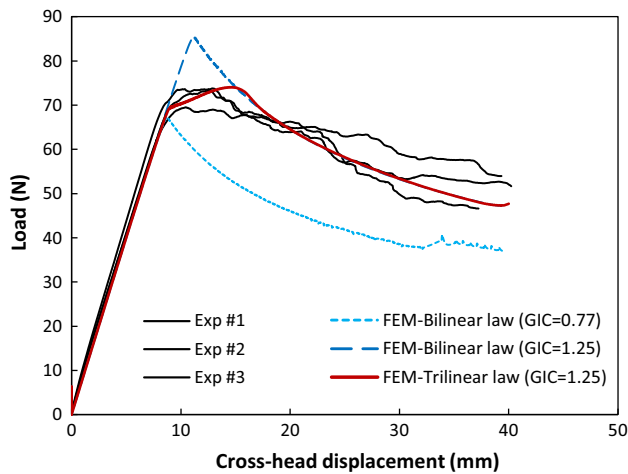


Figure 8 Force–displacement response of DCB test specimen of unstitched UD flax fiber composite; FEM and experimental results.

onset is captured with good accuracy. However, the model is not able to predict the force response during delamination propagation and the overall force response is underestimated. On the other hand, using the steady-state G_{IC} value [denoted by ‘FEM-Bilinear law ($G_{IC} = 1.25$)’] overestimates the failure loads in the early period of crack growth that most likely coincides with the development of the fiber bridging zone. Nevertheless, it is able to capture the delamination propagation response in the presence of fiber bridging traction which acts over the extended damage zone in the wake of the crack tip. These results thereby confirm that the use of a bilinear law to model delamination in the presence of extensive fiber bridging (Fig. 7) can introduce severe inaccuracy to the prediction of failure loads during DCB test.

Conversely, the use of the trilinear cohesive law [denoted by ‘FEM-Trilinear law ($G_{IC} = 1.25$)’] gave a good approximation to the experimental load–displacement curve. The nonlinear softening law is able to predict the onset of nonlinearity of the loading curve corresponding to the physical onset as well as the propagation of delamination. Generally, in the presence of fiber bridging, the damage process zone is extended by inducing bridging traction over the wake of the crack tip, which leads to significant increase in the crack growth resistance of fiber-reinforced composites. Therefore, the use of nonlinear softening law is necessary to differentiate decohesion of the matrix at the crack tip from bridging traction in the crack wake.

The experimental R-curve is compared with the predicted results from the FE analysis in Fig. 9. Similar to the experimental data reduction method (i.e., MBT), the Irwin–Kies equation was used to calculate the Mode I critical strain energy release rate, G_{IC} , of the FE analysis. The numerical results indicate that the trilinear law is able to predict the initiation and the final steady-state values of experimental G_{IC} very well. However, the experimental R-curve hits a peak G_{IC} before reaching steady-state propagation, which is not predicted in the FE analysis results. This is because the trilinear cohesive law parameters of m and n were calculated based on the average steady-state G_{IC} value of 1.25 kJ m^{-2} . As discussed previously, this value was chosen so as to cover a representative set of steady-state data points from the experimental R-curve. It was shown [35] that the shape of R-curve, i.e., the relation between the G_{IC} and the crack length, was not material property and depended on specimen geometry once large-scale fiber bridging occurs across the delamination plane. However, the initiation and steady-state values of Mode I critical strain energy release rate (G_{IC}) were found to be independent of specimen geometry. The trilinear cohesive law obtained by this method was therefore employed as the interlaminar response of the parent laminate to model the delamination of stitched laminates.

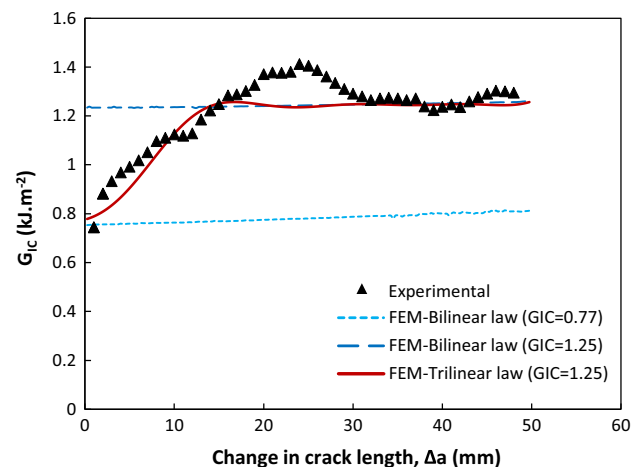


Figure 9 Experimental R-curve and FE analysis results of bilinear and trilinear cohesive laws.

Results of FEM modeling of DCB testing of stitched composite

The force–displacement response of the simulation of the stitched UD flax fiber composite is plotted against the experimental results in Fig. 10. The DCB tests of the stitched UD composite exhibit unstable crack growth followed by arrest, giving rise to stick–slip response in the load–displacement curves. Here, the experimental curves are intended to provide an indication of the dispersion of the onset of the stick–slip crack propagation due to variation in the properties of stitch yarns as well as the stitching distribution.

As it can be seen, the FE model shows reasonably good agreement with the experimental responses. Although the first stick–slip onset fracture point is different, the predicted response in terms of the peak and crack arresting loads, as well as the linear behavior of the load–displacement curve, is within the range of the experimental results. The slope is characteristic of DCB specimens due to the change in arm compliance as the effective arm length increases. The regularity of the stick–slip crack growth in both numerical and experimental results suggests that the behavior is intrinsically linked to the strain energy build up and release events induced by the stitch reinforcements.

A number of explanations can be offered for the discrepancy between the experimental and predicted force–displacement response. First, some variation in thickness of the DCB specimen arms which can occur

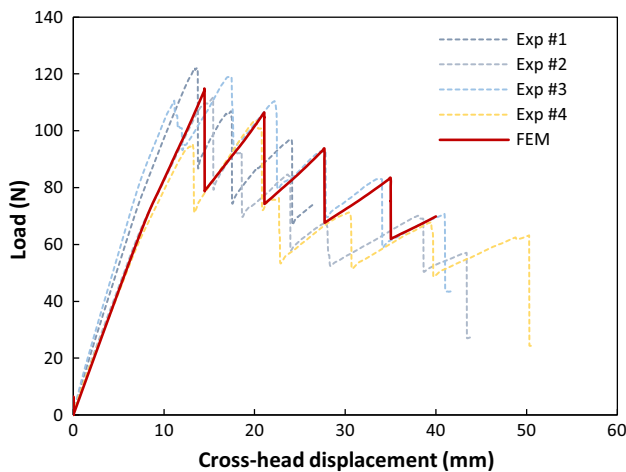


Figure 10 Force–displacement response of DCB test specimen of stitched UD flax fiber composite; experimental versus FEM analysis results.

with the resin infusion manufacturing method leads to some variations in the initial stiffness of the specimens (before crack initiation).

Second, the discrepancy in the stick–slip responses is also attributable to the small local variations in the stitch punching locations and distribution. In practice, actual stitch parameters (stitch length and row spacing) do deviate from the nominal values used in the numerical simulation (see Fig. 1) due to hand-stitching of the fiber preform.

Third, the variation could also have arisen from the properties assigned to the stitch elements, as the consistency and properties of natural fibers can often vary by up to 25–30%. A parametric sensitivity study of tensile properties of the stitch fibers is given in next section. However, despite these discrepancies, the predicted response is considered to be reasonably representative.

Figure 11 compares the predicted Mode I critical strain energy release rate of the stitched DCB model with the experimental values of G_{IC} with an identical stitch areal fraction. It is noteworthy that the stitch areal fraction, despite the plausible variation in the stitch distribution caused by hand-stitching, remains unchanged in all the test specimens.

The results of Fig. 11 indicate that the prediction of the stick–slip initiation G_{IC} values by the FEM analysis do give a reasonable representation of the average of the experimental values for the stitched composites. The virtual DCB test also exhibits the R-curve response, ramping from initiation $G_{IC} = 1.3(\text{kJ m}^{-2})$ to the constant stick–slip propagation

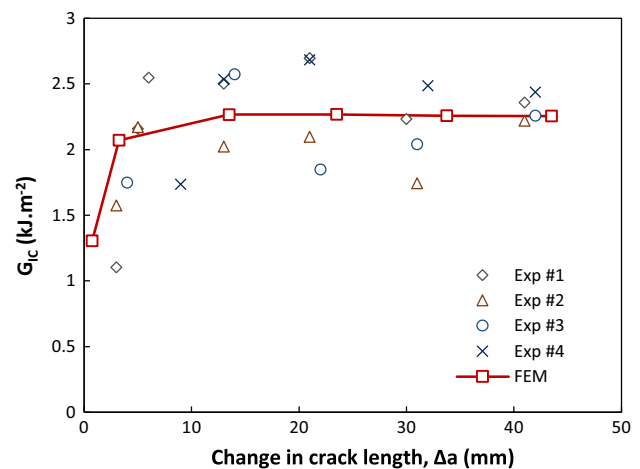


Figure 11 Experimental and FE analysis R-curve of stitched UD flax fiber composite.

values of $G_{IC} = 2.26(\text{kJ m}^{-2})$, which agree with the average of the experimental results very well. The average experimental values were $G_{IC} = 1.34(\text{kJ m}^{-2})$ and $G_{IC} = 2.22(\text{kJ m}^{-2})$ for initiation and stick–slip propagation, respectively. It is now confirmed experimentally and with FE prediction that stitching with twistless flax yarn can enhance the average interlaminar fracture toughness from $G_{IC} = 1.25(\text{kJ m}^{-2})$ for unstitched laminates to $G_{IC} = 2.26(\text{kJ m}^{-2})$ for the flax yarn stitched composites, i.e., an improvement of 80%.

The evolution of the crack length against the crosshead opening displacement obtained by experimental and FE simulation of un/stitched DCB test specimens is compared in Fig. 12. The model appears to be able to give a satisfactory prediction of interlaminar failure of the unstitched and stitched specimens. The fit between the predicted and experimental crack lengths for the unstitched composites is very good. This means that for any given values of crack length, the numerical compliance ($P \cdot \delta^{-1}$) accurately matches the experimental values.

For the stitched model, despite the discrepancy between the crack arrest lengths, the numerical model shows that the crack growth takes place at a similar rate to the experimental data. As discussed above, the difference between the predicted crack length and the experimental data, against the crosshead opening displacement, is attributable to the discrepancy in stitch punching locations between the actual specimens and the numerical model as well as

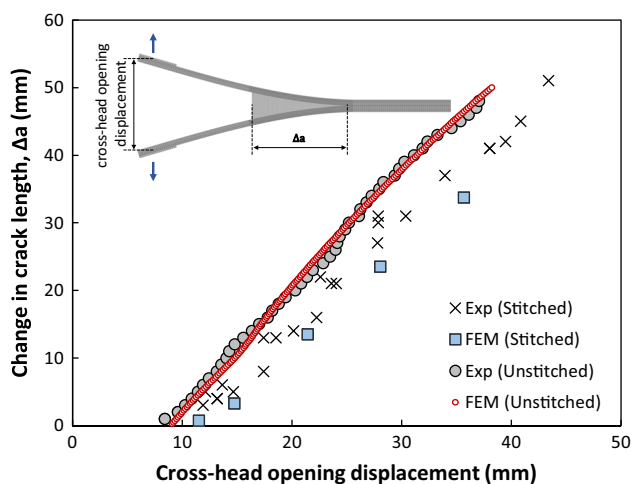


Figure 12 Change in crack length against crosshead opening displacement for experimental and FE analysis.

intrinsic variation in the tensile properties of the stitch fibers. It is worth mentioning that due to stick–slip crack growth, only the crack arrest length and the associated maximum opening displacement are plotted for the stitched composites.

Figure 13 compares the delamination growth threshold markings on the numerical and experimental load–displacement curves of the stitched composites (i.e., point 1, 2 and 3). As can be seen, there is a good agreement between the calculated and the measured curves. The numerical model is able to accurately predict the bilinear rise in the force in the elastic region, the peak force as well as the force jagged pattern due to the stick–slip crack growth.

In the DCB test, the opening force of the specimen's arms is linear till it reaches the point 1, as shown in Fig. 13. This point indicates the onset of delamination from the end of the PTFE insert (pre-crack) in the both unstitched and stitched composites (Fig. 14a). Beyond point 1, unlike the stable crack propagation in the unstitched composite, the linear force rise continues in the stitched composite while the gradient is slightly changed compared to the earlier part. At this step, the crack passes round the stitch fiber and is arrested behind the stitch line while the stitch fibers are bridging the crack, as shown in the damage evolution of the cohesive layer of the DCB test model in Fig. 14b. The opening force then rises to a maximum value at point 2, where the failure stress of stitch elements is reached. Finally, the stitch elements fracture and the force drops abruptly till stops at point 3, while the force is always above the failure force of the unstitched composite. Releasing the stored strain energy in the stitch elements causes the crack to propagate at higher speeds toward the vicinity of the next stitch line, as shown in Fig. 14c. This progressive failure is repeated for each stitch line and leads to the unstable stick–slip crack growth behavior observed experimentally.

Parametric study

It was discussed in the previous section that variation in the tensile properties of stitch yarn, i.e., flax yarn, can explain the discrepancy between the predicted and measured values of the Mode I interlaminar fracture toughness of the stitched composite. It is rather clear that the strength of the stitch material is the most important parameter and has a significant influence on the bridging traction and on the

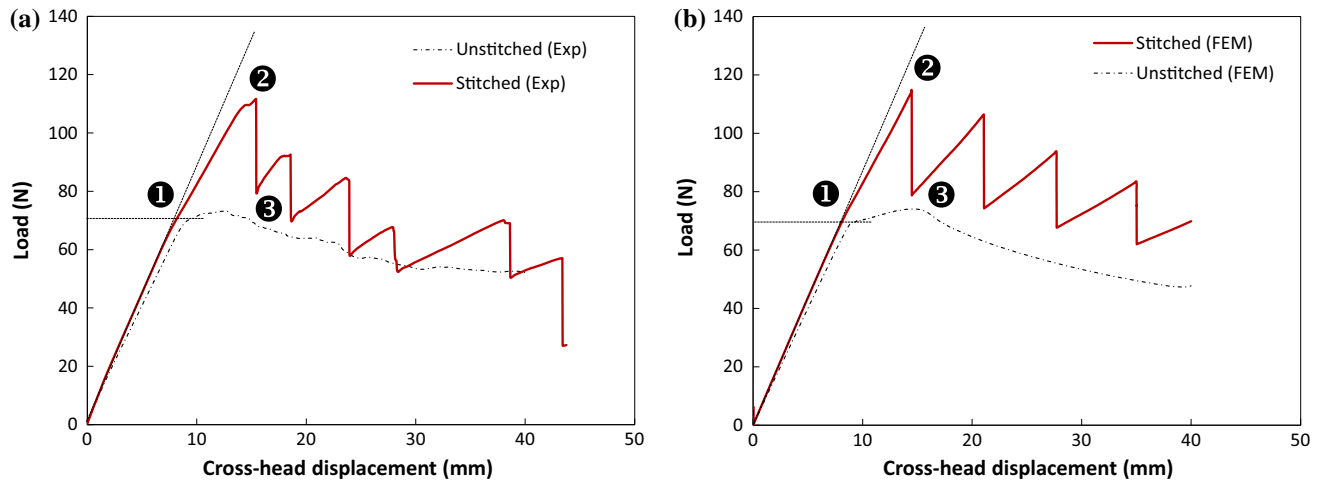


Figure 13 Three-step delamination growth marking on the load–displacement curve of DCB test of stitched composite; comparison of **a** experimental results with **b** predicted results.

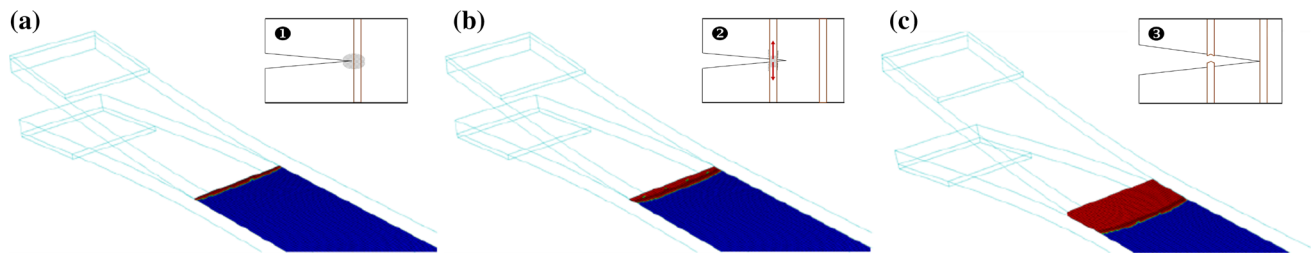


Figure 14 Interlaminar damage (delamination) evolution within the stitched UD flax fiber composite; **a** the cohesive interface failure propagates and passes round the stitch elements, **b** the crack then is arrested behind the stitch elements while the stitch elements

are stretched, **c** the stitch elements fracture, and the stored energy is released to propagate the cohesive crack at higher speed until the next row of stitch elements.

delamination resistance accordingly. In this regard, a parametric study was performed to determine the effect of the tensile strength, X_t^{stitch} , of the stitch yarn on the delamination resistance of the stitched UD flax fiber composite.

The experimental study on the tensile properties of the flax yarn showed a coefficient of variation of 25–30% for the tensile strength of the impregnated flax yarn [38]. Here, we consider two extreme values for the strength of the stitch elements in which they are 15% above and below the average value of the strength used in FEM analysis in previous section (i.e., $X_t^{stitch} = 380\text{MPa}$ and $X_t^{stitch} = 280\text{MPa}$ for the maximum and minimum values of the strength, respectively).

The effect of variation of stitch strength on the interlaminar fracture toughness (G_{IC}) is shown in Fig. 15. A variation of 30% in the strength of stitch elements leads to 20 and 31% change in the peak force and the propagation value of G_{IC} , respectively.

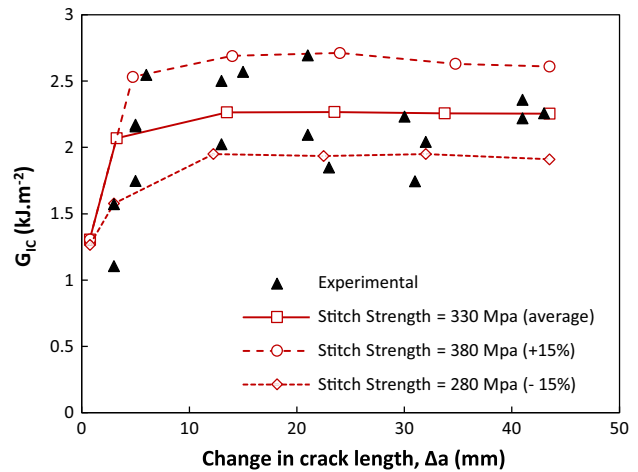


Figure 15 Effect of variation of stitch strength on R-curve of the stitched UD flax fiber composite.

This is an indication of the sensitivity of Mode I interlaminar fracture toughness to the bridging traction taking place across the delamination plane. In

other words, any variation in the strength of the stitch material would be reflected in the toughness adding to the composite. It is apparent from the Fig. 15 that the majority of the experimental data fall between the numerically predicted upper and lower limits. As a result, it can be said that the dispersion in the experimentally measured values of G_{IC} is mainly attributable to the variation in the strength of the stitch yarn.

Conclusion

The effect of introducing out-of-plane flax fiber stitches on the Mode I interlaminar fracture toughness of the UD flax/epoxy composites was experimentally and numerically investigated. The DCB test results for the unstitched flax fiber composites showed a strong R-curve effect, which was attributed to the large-scale in-plane fiber bridging, observed during delamination advancement. The experimental findings also showed that the use of twistless flax yarn stitches was effective and can improve the Mode I critical strain energy release rate at by around 78% to over 2 kJ m^{-2} .

In the FE analysis, a cohesive element with trilinear cohesive law obtained from the superposition of two bilinear cohesive laws was used to model the R-curve effect. It was shown that this approach is accurate enough to capture the initiation and steady-state propagation values of G_{IC} of the R-curve induced by the large-scale in-plane fiber bridging. The resultant cohesive interface was then superposed with beam elements as the stitch fibers to simulate the delamination of stitched laminate in the presence of extensive in-plane fiber bridging. The stitch model was built based on experimental observations in which the fracture of stitches was found to occur at the delamination plane with no slippage effect at the embedded end. The FE results showed reasonably good agreement with the experimental results and the prediction of the Mode I critical strain energy release rate for the initiation and propagation phase of the delamination was within the range of the measured values. Moreover, the parametric study on the strength of the stitch yarn showed that the variation in the measured values of G_{IC} was in line with the dispersion of strength of the stitch yarn. The results of this work suggest that stitching is a promising technique to enhance the interlaminar

fracture toughness of flax/epoxy composite laminates, and it is crucial to consider the effects of in-plane fiber bridging to have an accurate characterization of G_{IC} values for stitched natural fiber composites.

The results of this study can help to deepen the understanding of the material behavior and interlaminar fracture mechanism of through-the-thickness reinforced flax fiber composites, which will assist in the development of engineering applications for the natural fiber composites.

Acknowledgements

The authors are grateful to the Agency for Science, Technology and Research (A*STAR), Singapore Institute of Manufacturing Technology, and the National University of Singapore for financial support (partially through Grant No. WBS R265000523646).

Compliance with ethical standards

Conflict of interest The authors declare that they have no conflict of interest.

References

- [1] Shah DU (2014) Natural fibre composites: comprehensive Ashby-type materials selection charts. *Mater Des* 62:21–31. <https://doi.org/10.1016/j.matdes.2014.05.002>
- [2] Müssig J, Haag K (2015) 2—the use of flax fibres as reinforcements in composites. In: Faruk O, Sain M (eds) *Biofiber reinforcements in composite materials*. Woodhead Publishing, Cambridge, pp 35–85
- [3] Faruk O, Sain M (2014) *Biofiber reinforcements in composite materials*. Elsevier, Amsterdam
- [4] Khanlou HM, Woodfield P, Summerscales J, Hall W (2017) Consolidation process boundaries of the degradation of mechanical properties in compression moulding of natural-fibre bio-polymer composites. *Polym Degrad Stab* 138:115–125. <https://doi.org/10.1016/j.polymdegradstab.2017.03.004>
- [5] Khanlou HM, Hall W, Heitzman MT et al (2016) Technical note: on modelling thermo-chemical degradation of poly(lactic acid). *Polym Degrad Stab* 134:19–21. <https://doi.org/10.1016/j.polymdegradstab.2016.09.033>
- [6] Bensadoun F, Verpoest I, Baets J et al (2017) Impregnated fibre bundle test for natural fibres used in composites. *J Reinf Plast Compos*. <https://doi.org/10.1177/0731684417695461>

- [7] Yan L, Chouw N, Jayaraman K (2014) Flax fibre and its composites—a review. *Compos B Eng* 56:296–317. <https://doi.org/10.1016/j.compositesb.2013.08.014>
- [8] Pickering K (2008) Properties and performance of natural-fibre composites. Elsevier, Boca Raton
- [9] Hodzic A, Shanks R (2014) Natural fibre composites: materials, processes and properties. Woodhead Publishing, Cambridge
- [10] Faruk O, Bledzki AK, Fink H-P, Sain M (2012) Biocomposites reinforced with natural fibers: 2000–2010. *Prog Polym Sci* 37:1552–1596. <https://doi.org/10.1016/j.progpolymsci.2012.04.003>
- [11] Shah DU, Schubel PJ, Clifford MJ (2013) Can flax replace E-glass in structural composites? A small wind turbine blade case study. *Compos B Eng* 52:172–181. <https://doi.org/10.1016/j.compositesb.2013.04.027>
- [12] Ravandi M, Teo WS, Tran LQN et al (2017) Low velocity impact performance of stitched flax/epoxy composite laminates. *Compos B Eng* 117:89–100. <https://doi.org/10.1016/j.compositesb.2017.02.003>
- [13] Zhong Y, Tran LQN, Kureemun U, Lee HP (2017) Prediction of the mechanical behavior of flax polypropylene composites based on multi-scale finite element analysis. *J Mater Sci* 52:4957–4967. <https://doi.org/10.1007/s10853-016-0733-7>
- [14] Kureemun U, Ravandi M, Tran LQN et al (2018) Effects of hybridization and hybrid fibre dispersion on the mechanical properties of woven flax-carbon epoxy at low carbon fibre volume fractions. *Compos B Eng* 134:28–38. <https://doi.org/10.1016/j.compositesb.2017.09.035>
- [15] Goutianos S, Peijs T (2003) The optimisation of flax fibre yarns for the development of high-performance natural fibre composites. *Adv Compos Lett* 12:237–241
- [16] Goutianos S, Peijs T, Nystrom B, Skrifvars M (2006) Development of flax fibre based textile reinforcements for composite applications. *Appl Compos Mater* 13:199–215
- [17] Dai S-C, Yan W, Liu H-Y, Mai Y-W (2004) Experimental study on z-pin bridging law by pullout test. *Compos Sci Technol* 64:2451–2457
- [18] Qiao Y (2003) Fracture toughness of composite materials reinforced by debondable particulates. *Scr Mater* 49:491–496
- [19] Sela N, Ishai O (1989) Interlaminar fracture toughness and toughening of laminated composite materials: a review. *Composites* 20:423–435
- [20] Ansar M, Xinwei W, Chouwei Z (2011) Modeling strategies of 3D woven composites: a review. *Compos Struct* 93:1947–1963
- [21] Suppakul P, Bandyopadhyay S (2002) The effect of weave pattern on the mode-I interlaminar fracture energy of E-glass/vinyl ester composites. *Compos Sci Technol* 62:709–717
- [22] Mouritz AP, Cox BN (2000) A mechanistic approach to the properties of stitched laminates. *Compos A Appl Sci Manuf* 31:1–27. [https://doi.org/10.1016/S1359-835X\(99\)00056-1](https://doi.org/10.1016/S1359-835X(99)00056-1)
- [23] Iwahori Y, Ishikawa T, Hayashi Y, Watanabe N (2000) Study of interlaminar fracture toughness improvement on stitched CFRP laminates. *J Jpn Soc Compos Mater (Japan)* 26:90–100
- [24] Shu D, Mai Y-W (1993) Effect of stitching on interlaminar delamination extension in composite laminates. *Compos Sci Technol* 49:165–171
- [25] Jain LK, Mai Y-W (1994) On the effect of stitching on Mode I delamination toughness of laminated composites. *Compos Sci Technol* 51:331–345. [https://doi.org/10.1016/0266-3538\(94\)90103-1](https://doi.org/10.1016/0266-3538(94)90103-1)
- [26] Massabo R, Cox BN (1999) Concepts for bridged Mode II delamination cracks. *J Mech Phys Solids* 47:1265–1300. [https://doi.org/10.1016/S0022-5096\(98\)00107-0](https://doi.org/10.1016/S0022-5096(98)00107-0)
- [27] Sun X, Tong L, Wood MDK, Mai Y-W (2004) Effect of stitch distribution on Mode I delamination toughness of laminated DCB specimens. *Compos Sci Technol* 64:967–981. <https://doi.org/10.1016/j.compscitech.2003.07.004>
- [28] Tsai G-C, Chen J-W (2005) Effect of stitching on Mode I strain energy release rate. *Compos Struct* 69:1–9. <https://doi.org/10.1016/j.compstruct.2004.02.009>
- [29] Iwahori Y, Nakane K, Watanabe N (2009) DCB test simulation of stitched CFRP laminates using interlaminar tension test results. *Compos Sci Technol* 69:2315–2322
- [30] Tan KT, Watanabe N, Sano M et al (2010) Interlaminar fracture toughness of vectran-stitched composites—experimental and computational analysis. *J Compos Mater* 44:3203–3229
- [31] Wood MDK, Sun X, Tong L et al (2007) The effect of stitch distribution on Mode I delamination toughness of stitched laminated composites—experimental results and FEA simulation. *Compos Sci Technol* 67:1058–1072. <https://doi.org/10.1016/j.compscitech.2006.06.002>
- [32] Heß H, Himmel N (2011) Structurally stitched NCF CFRP laminates. Part 2: finite element unit cell based prediction of in-plane strength. *Compos Sci Technol* 71:569–585
- [33] Sankar BV, Dharmapuri SM (1998) Analysis of a stitched double cantilever beam. *J Compos Mater* 32:2203–2225. <https://doi.org/10.1177/002199839803202402>
- [34] Chen L, Ifju PG, Sankar BV (2005) Analysis of Mode I and Mode II tests for composites with translaminar reinforcements. *J Compos Mater* 39:1311–1333. <https://doi.org/10.1177/0021998305050425>
- [35] Sørensen BF, Jacobsen TK (1998) Large-scale bridging in composites: R-curves and bridging laws. *Compos A Appl*

- Sci Manuf 29:1443–1451. [https://doi.org/10.1016/S1359-835X\(98\)00025-6](https://doi.org/10.1016/S1359-835X(98)00025-6)
- [36] Airoidi A, Dávila CG (2012) Identification of material parameters for modelling delamination in the presence of fibre bridging. *Compos Struct* 94:3240–3249. <https://doi.org/10.1016/j.compstruct.2012.05.014>
- [37] Dávila CG, Rose CA, Camanho PP (2009) A procedure for superposing linear cohesive laws to represent multiple damage mechanisms in the fracture of composites. *Int J Fract* 158:211–223. <https://doi.org/10.1007/s10704-009-9366-z>
- [38] Ravandi M, Teo WS, Tran LQN et al (2016) The effects of through-the-thickness stitching on the Mode I interlaminar fracture toughness of flax/epoxy composite laminates. *Mater Des* 109:659–669. <https://doi.org/10.1016/j.matdes.2016.07.093>
- [39] D30 Committee (2007) Test method for Mode I interlaminar fracture toughness of unidirectional fiber-reinforced polymer matrix composites. ASTM International, West Conshohocken
- [40] Tamuzs V, Tarasovs S, Vilks U (2001) Progressive delamination and fiber bridging modeling in double cantilever beam composite specimens. *Eng Fract Mech* 68:513–525. [https://doi.org/10.1016/S0013-7944\(00\)00131-4](https://doi.org/10.1016/S0013-7944(00)00131-4)
- [41] Sørensen BF, Goutianos S, Jacobsen TK (2009) Strength scaling of adhesive joints in polymer–matrix composites. *Int J Solids Struct* 46:741–761. <https://doi.org/10.1016/j.ijsolstr.2008.09.024>
- [42] Boyang C (2013) Numerical modelling of scale-dependent damage and failure of composites. Ph.D
- [43] Turon A, Dávila CG, Camanho PP, Costa J (2007) An engineering solution for mesh size effects in the simulation of delamination using cohesive zone models. *Eng Fract Mech* 74:1665–1682. <https://doi.org/10.1016/j.engfracmech.2006.08.025>
- [44] Chen BY, Tay TE, Baiz PM, Pinho ST (2013) Numerical analysis of size effects on open-hole tensile composite laminates. *Compos A Appl Sci Manuf* 47:52–62. <https://doi.org/10.1016/j.compositesa.2012.12.001>
- [45] Lampani L (2011) Finite element analysis of delamination of a composite component with the cohesive zone model technique. *Eng Comput* 28:30–46. <https://doi.org/10.1108/02644401111097000>
- [46] Camanho PP, Dávila CG (2002) Mixed-mode decohesion finite elements for the simulation of delamination in composite materials. NASA-technical paper 211737, p. 33
- [47] Dassault Systèmes Simulia Corp (2011) Abaqus 6.11 documentation. Dassault Systèmes, Providence, RI, USA
- [48] Ravandi M, Teo WS, Tran LQN, Tay MSY and TE (2016) Mode I interlaminar fracture toughness of natural fiber stitched flax/epoxy composite laminates—experimental and numerical analysis. In: Proceedings of the American society for composites: thirty-first technical conference
- [49] Popelar CH, Kanninen MF (1985) Advanced fracture mechanics, 1st edn. Oxford University Press, New York
- [50] Manshadi BD, Farmand-Ashtiani E, Botsis J, Vassilopoulos AP (2014) An iterative analytical/experimental study of bridging in delamination of the double cantilever beam specimen. *Compos A Appl Sci Manuf* 61:43–50. <https://doi.org/10.1016/j.compositesa.2014.02.001>